SIMULATION OF GROWTH KINETICS OF Fe$_2$B LAYERS FORMED ON GRAY CAST IRON DURING THE POWDER-PACK BORIDING

SIMULACIJA KINETIKE RASTI PLASTI Fe$_2$B NA SIVEM LITEM ŽELEZU PRI BORIRANJU S PRAHOM V PAKETU

Martin Ortiz-Domínguez[1], Miguel Ángel Flores-Rentería[1], Mourad Keddam[2], Milton Elias-Espinosa[3], Omar Damián-Mejía[4], Jorge Iván Aldana-González[5], Jorge Zuno-Silva[1], Sergio Alejandro Medina-Moreno[6], José Gonzalo González-Reyes[4]

[1]Escuela Superior de Ciudad Sahagún, Universidad Autónoma del Estado de Hidalgo, UAEH, Carretera Cd. Sahagún-Otumba s/n, 43990 Hidalgo, México
[2]USTHB, Faculté de Génie Mécanique et Génie des Procédés, Laboratoire de Technologie des Matériaux, B.P. No. 32, 16111 El-Alia, Bab-Ezzouar, Algiers, Algeria
[3]Instituto Tecnológico y de Estudios Superiores de Monterrey-ITESM Campus Santa Fe, Av. Carlos Lazo No. 100, Del. Álvaro Obregón, CP. 01389, México, D. F.
[4]Universidad Nacional Autónoma de México-UNAM, Instituto de Investigación en Materiales, Circuito Exterior, s/n Ciudad Universitaria, Coyoacán, CP 04510, México, D. F.
[5]Universidad Tecnológica de México, Blvd. Calacoaya No. 7, Col. La Ermita Atizapán de Zaragoza, Estado de México, 52970, Estado de México, México
[6]Universidad Politécnica de Pachuca-UPP, Carretera-Cd. Sahagún km. 20, Ex Hacienda de Santa Bárbara, CP 43830, Hidalgo, México
keddam@yahoo.fr

The modeling of the growth kinetics of boride layers is an important tool determining suitable process parameters for obtaining an adequate boride-layer thickness. In this study, a mathematical model of the growth kinetics of the Fe$_2$B layers on gray cast iron was proposed for the powder-pack boriding. The kinetic-diffusion model considers the mass balance equation of the (Fe$_2$B/Fe) interface with the purpose of determining the boron diffusion coefficients (D_{Fe_2B}) in the Fe$_2$B layers. The kinetic model was set for the Fe$_2$B layer thickness, assuming that the growth of boride layers follows a parabolic growth law. The presented model can be used to predict the Fe$_2$B layer thickness formed on gray cast iron during the powder-pack boriding. This process was carried out in the temperature range of 1123–1273 K with the exposure times ranging from 2 h to 8 h. The reliability of the technique used is compared with the experimental value for the Fe$_2$B layer thickness obtained at 1253 K after 5 h of treatment time. The X-ray diffraction method (XRD), the energy dispersive spectroscopy (EDS) and the adherence of the layer/substrate were applied.

Keywords: boriding, incubation time, diffusion model, growth kinetics, activation energy, adherence

Modeliranje kinetike rasti boridnih plasti je pomembno orodje za določanje primernih parametrov procesa nastanka primerne debeline plasti borida. V tej študiji je predlagan matematični model kinetike rasti plasti Fe$_2$B na sivem litem železu pri boriranju s prahom v paketu. Namen kinetičnega difuzijskega modela, ki upošteva enačbo masne balance na stiku (Fe$_2$B/Fe) je določanje koeficienta difuzije bora (D_{Fe_2B}) v plasti Fe$_2$B. Kinetični model je bil postavljen za debelino plasti Fe$_2$B in s predpostavko, da boridna plast raste po paraboličnem zakonu. Predstavljeni model se lahko uporabi za napovedovanje debeline plasti Fe$_2$B na sivem litem železu pri boriranju s prahom v paketu. Ta postopek je bil izvršen v območju temperatur 1123–1273 K s trajanjem od 2 h do 8 h. Zanesljivost uporabljene tehnike je bila primerjana z eksperimentalno vrednostjo plasti Fe$_2$B pri 1253 K po 5 h obdelave. Uporabljene so bile metode uklona rentgenskih žarkov (XRD), energijska disperzijska spektroskopija (EDS) in oprijemljivost plasti na podlagi.

Ključne besede: boriranje, čas inkubacije, difuzijski model, kinetika rasti, aktivacijska energija, oprijemljivost

1 INTRODUCTION

The maximum protection against wear and corrosion is becoming more and more important for a wide range of components. Apart from the construction materials that meet these high requirements, processes have been developed with a positive effect on the wear and corrosion resistance of a component surface. For the thermochemical treatment of steel, nitriding, surface and case hardening and boriding are the most important processes in use. At the beginning of the previous century it became apparent that extremely hard and wear-resistant surfaces could be obtained with a diffusion of boron atoms into steel surfaces. Theoretically, liquid, gaseous and solid media can be used to supply boron atoms[1–3].

However, due to the difficulties with regard to the process technology, boriding in salt melts and out of the gas phase has still not gained ground. Also, the development of plasma boriding is still at the testing stage. At present, the only process that is economical in practice is boriding in solid media with variants. Boride layers are particularly beneficial to the components submitted to abrasive wear and have a number of special advantages over the conventional case-hardened layers, such as an extremely high hardness (between 1600 HV and 2000 HV)[4–8]. Also, the combination of a high surface hardness and a low surface coefficient of friction of a boride layer makes a significant contribution to combat the main wear mechanisms: adhesion, tribo-oxidation, abrasion and

surface fatigue. This fact has enabled the mold makers to substitute easier-to-machine steels for the base metal and to still obtain the wear resistance and anti-galling properties superior to those of the original material. The hardness of a boride layer can be retained at higher temperatures. Boriding can considerably enhance the corrosion-erosion resistance of ferrous materials in non-oxidizing dilute acids and alkali media, and it is increasingly used due to this advantage in many industrial applications[7].

The term boriding means the enrichment of the surface of a workpiece with boron atoms with thermo-chemical treatment. Generally, the growth kinetics of solid phases is controlled with the diffusion of elements in theses phases[1]. The displacement speed of interfaces is analyzed in dependence of diffusion fluxes of elements to and from these interfaces. It is assumed that the balance of diffusion fluxes of diffusion elements (penetrating into an individual phase and leaving this phase) determines the growth (or reduction) of the layers of the phases and their thicknesses. If only one element is negligible and small with respect to the first element, the balance of diffusion fluxes is reduced to the arrival and the departure of the element at the phase interface[9]. By means of thermal energy, boron atoms are transferred into the lattice of the parent material, forming the respective borides. The boriding of steel alloys results in a formation of either a single-phase or a double-phase layer of boride with definite compositions. A single-phase boride layer consists of Fe₂B (containing approximately 60×10^3 mol m⁻³ of boron), while a double-phase layer consists of an outer phase of FeB (containing approximately 100×10^3 mol m⁻³ of boron) and an inner phase of Fe₂B[10]. The FeB phase is brittle and forms a highly tensile-stressed surface. The Fe₂B phase is preferred because it is less brittle and forms a surface with a high compressive stress. The thickness of the boride layer formed depends on the temperature and the treatment time[9–20]. Although small amounts of FeB are present in most boride layers, they are not detrimental if not continuous. However, a continuous layer of FeB can lead to crack formation at the (FeB/Fe₂B) interface. Furthermore, since the FeB and Fe₂B phases exhibit substantially different coefficients of thermal expansion ($\alpha_{FeB} = 8.4 \cdot 10^{-8}$ K⁻¹, $\alpha_{Fe_2B} = 2.9 \cdot 10^{-8}$ K⁻¹) in the temperature range of 473–873 K, crack formations are often observed at the (FeB/Fe₂B) interface of a double-phase layer. These cracks can lead to a separation of spalling of a double-phase layer when a mechanical strain is applied or when the component is submitted to a thermal and/or a mechanical shock[2]. Fortunately, continuous layers of FeB can be minimized by diffusion annealing after boride formation[9,21]. Also, the boriding powders that minimize the formation of FeB have been developed and are available. The preferred morphology is a sawtooth of the serrated-boride-layer structure, most easily obtained with carbon or low-alloy steels[3,10,17,22,23]. The micro-hardness of a boride layer also depend strongly on the composition and structure of the boride layer and of the

base material. In practical applications of boriding, the selection of process parameters is important in order to attain the desired thickness of a boride layer and a hardness gradient. The thickness of a boride layer that affects the mechanical and chemical behavior of a material depends on the boriding temperature, the boriding time, the active-boron quantity at a sample surface and the chemical composition of the material[10,12,23]. Therefore, estimating the kinetics parameters of developing boride layers during the boriding process is crucial. The growth kinetics of iron boride layers has received a particular interest in the field of boriding treatment in order to automate and optimize the process. For this reason, different mathematical models have been proposed to determine the boron diffusion coefficients of borides[5,8,10,16,18,19,22–25]. Most of these models consider the thermodynamic equilibrium at the interface during the growth and a linear boron-concentration profile for the boride layer. Nevertheless, mathematical models are sensitive to the experimentally obtained boride-layer thickness, which is the main reason for a lack of data about boron diffusion coefficients for boride layers. Likewise, the dependence of the temperature and boron diffusion coefficient can be deducted with the Arrhenius equation, which makes it possible to calculate the boron diffusion activation energy (Q_{Fe_2B}). In this study the boriding of the surface of gray cast iron hardened during the powder-pack process is analyzed on the basis of the growth kinetics of the Fe₂B layers formed on the surface of gray cast iron due to powder-pack boriding. The parabolic growth constants of Fe₂B were determined and the boron diffusion coefficient for the boride layer was estimated using a diffusion model based on the conditions of the boriding process and the Fe-B system. Moreover, X-ray diffraction (XRD), scanning electron microscopy (SEM) and energy dispersive X-ray spectroscopy (EDS) were conducted on the borided material to characterize the presence of the Fe₂B layer and the distribution of heavy elements on the surface of gray cast iron. In addition, the Daimler-Benz Rockwell-C indentation tests were also applied (prescribed by the VDI 3198 norm) exhibiting distinct properties of the coated compound, i.e., interfacial adhesion, coating brittleness and cohesion.

2 DIFFUSION MODEL

2.1 Mass-balance equation

The model considers a system in which a solute is added to the surface of a two-phase alloy with a composition of $C_0 \approx 0$ mol m⁻³. As boron is added to the surface, it is used completely to convert the Fe phase to Fe₂B. There is no boron flux out of the surface layer of Fe₂B into the two-phase alloy. The boron concentration along the depth of the sample surface is depicted in **Figure 1**.

The first step corresponds to a normal diffusion process before the formation of Fe₂B layers. For this period, labeled as time $t_0^{Fe_2B}$ in **Figure 1,** the boron
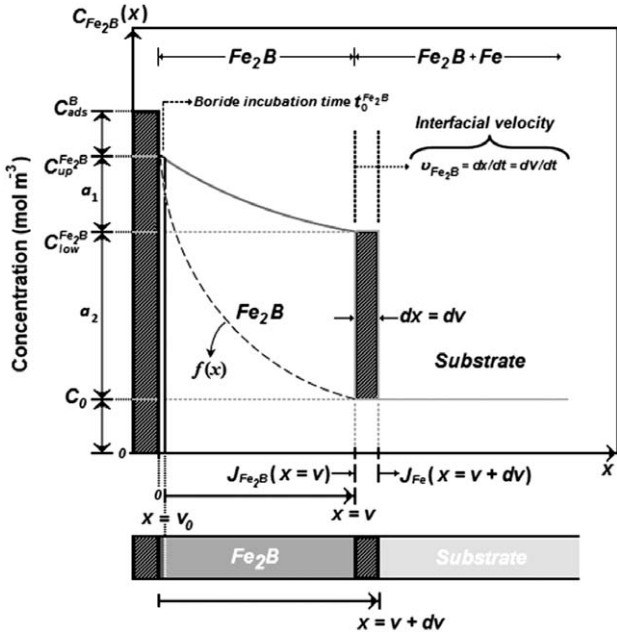
Figure 1: Boron concentration profile for the Fe₂B layer, $C_{\mathrm{up}}^{\mathrm{Fe_2B}}$ and $C_{\mathrm{low}}^{\mathrm{Fe_2B}}$ values obtained from the Fe-B phase diagram for a range of temperature

Slika 1: Profil koncentracije bora v plasti Fe₂B; vrednosti $C_{\mathrm{up}}^{\mathrm{Fe_2B}}$ in $C_{\mathrm{low}}^{\mathrm{Fe_2B}}$, dobljene iz faznega diagram Fe-B za območje temperatur

concentration profile in austenite corresponding to $f(x)$ and marked with a dashed line, is displayed in **Figure 1** (where $f(x)$ denotes the initial concentration profile when the layer formation begins). In the model, this is equivalent to the "supersaturated" austenite. In this period, the formation of compact layers begins to take place, as shown in **Figure 1**, where $C_{\mathrm{up}}^{\mathrm{Fe_2B}}$ is the upper limit of the boron amount in Fe₂B (= 60×10³ mol m⁻³), $C_{\mathrm{low}}^{\mathrm{Fe_2B}}$ is the lower limit of the boron amount in Fe₂B (= 59.8×10³ mol m⁻³) and point $x(t) = v$ width of the Fe₂B layer[9,10]. Note that in this case, the position of the discontinuity does not correspond to the thermodynamic-phase equilibrium associated with the limits of solubility of each phase in the Fe-B phase diagram. The boron concentration of the Fe₂B phase in equilibrium with austenite has its value determined on the basis of the intersection with $f(x)$ "supersaturated" austenite. The term $C_{\mathrm{ads}}^{\mathrm{B}}$ is the effective boron concentration or the adsorbed boron concentration in the boride layer during the boriding process[13]. On **Figure 1**, $a_1 = C_{\mathrm{up}}^{\mathrm{Fe_2B}} - C_{\mathrm{low}}^{\mathrm{Fe_2B}}$ defines the homogeneity range of the Fe₂B layer, $a_2 = C_{\mathrm{low}}^{\mathrm{Fe_2B}} - C_0$ is the miscibility gap and C_0 is the terminal solubility of the interstitial solute. The boron solubility in the austenite phase is very low and can be neglected by setting $C_0 \approx 0$ mol m⁻³.[26,27] Certain assumptions are considered in the establishment of the diffusion model:

a) The diffusion model was not based on the boron concentration profile $C_{\mathrm{Fe_2B}}[x(t)]$ of the Fe₂B layer (**Figure 1**).

b) The growth kinetics is controlled by the boron diffusion in the Fe₂B layer.

c) Fe₂B nucleates after a period of incubation.

d) The boride layer grows because of the boron diffusion perpendicular to the specimen surface.

e) Boron concentrations remain constant in the boride layer during the treatment.

f) The influence of the alloying elements on the growth kinetics of the layer is not taken into account.

g) The boride layer is thin compared to the sample thickness.

h) A uniform temperature throughout the sample is assumed.

i) A planar morphology is assumed for the phase interface.

With these assumptions, the initial and boundary conditions can be written as (**Figure 1**):

Initial condition:

$$t = 0,\ x > 0,\ \text{with: } C_{\mathrm{Fe_2B}}\,[x(t)] = C_0 \approx 0 \qquad (1)$$

Boundary conditions:

$$C_{\mathrm{Fe_2B}}\left[x(t = t_0^{\mathrm{Fe_2B}}) = v_0\right] = C_{\mathrm{up}}^{\mathrm{Fe_2B}} \qquad (2)$$

(The upper boron concentration is kept constant), for $C_{\mathrm{ads}}^{\mathrm{B}} > 60 \times 10^3$ mol m⁻³:

$$C_{\mathrm{Fe_2B}}\left[x(t = t) = v\right] = C_{\mathrm{low}}^{\mathrm{Fe_2B}} \qquad (3)$$

(The boron concentration at the interface is kept constant), for $C_{\mathrm{ads}}^{\mathrm{B}} < 59.8 \times 10^3$ mol m⁻³

where $t_{\mathrm{v}}\ (= t - t_0^{\mathrm{Fe_2B}})$ is the effective growth time of the Fe₂B layer, t is the treatment time, $t_0^{\mathrm{Fe_2B}}$ is the boride incubation time and v_0 the initial Fe₂B layer related with the initial period $t_0^{\mathrm{Fe_2B}}$ of the interaction of elementary substances (boron atoms and substrate) due to the presence of the Fe₂B layer. In addition, v_0 is a thin layer with a thickness of ≈ 5 nm formed during the nucleation stage.[28] However, the value of $v_0 \approx 0$ is small in comparison with the measured thickness of the Fe₂B layer (v) and it can, therefore, hardly have a noticeable effect on the shape of the layer thickness-time dependences observed in practice. Given the aforementioned conditions, it is taken into account that the boride-layer thickness v is governed by the parabolic growth law, $v = 2\varepsilon D_{\mathrm{Fe_2B}}^{1/2} t^{1/2} = 2\varepsilon D_{\mathrm{Fe_2B}}^{1/2}(t_{\mathrm{v}} + t_0^{\mathrm{Fe_2B}})^{1/2}$, where ε is the normalized growth parameter for the (Fe₂B/substrate) interface[29], and $D_{\mathrm{Fe_2B}}$ denotes the diffusion coefficient of boron in the Fe₂B phase. In an infinitesimally small time interval $\mathrm{d}t$ the growth of Fe₂B occurs due to a simultaneous consumption of the substrate at the (Fe₂B /substrate) interface boundary. Considering that $\mathrm{d}v$ (**Figure 1**) is an extension of the Fe₂B layer in a time interval ($\mathrm{d}t$) boron atoms should be conserved at the (Fe₂B/substrate) interface. Hence, applying the rule of mass conservation at the (Fe₂B/substrate) interface,[30,31]
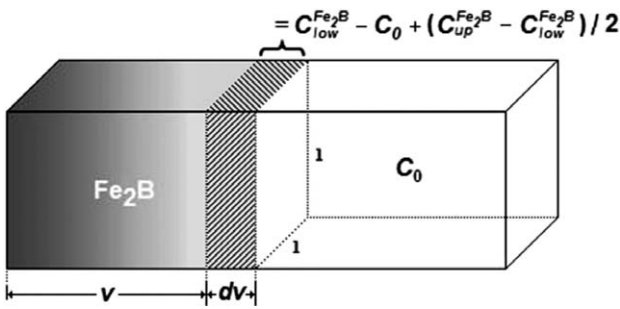
Figure 2: Schematic representation of the mass-balance equation at the (Fe₂B/substrate) interface
Slika 2: Shematski prikaz enačbe ravnotežja mas na stiku Fe₂B-podlaga

which is schematically represented in **Figure 2**, is defined as:

$$\left(\frac{C_{up}^{Fe_2B}+C_{low}^{Fe_2B}-2C_0}{2}\right)(A\cdot dv) = \tag{4}$$
$$=J_{Fe_2B}(x=v)(A\cdot dt)-J_{Fe}(x=v+dv)(A\cdot dt)$$

where A (=1·1) is defined as the unit area. Assuming that the diffusion of the metal component is negligible[16,24] nearly all the growth of the Fe₂B layer can be explained on the basis of the diffusivity of boron atoms. On the other hand, the input and output fluxes of boron atoms at the (Fe₂B/substrate) interface boundary in time interval dt are defined as:

$J_{Fe_2B}(x=v)=-\{D_{Fe_2B}dC_{Fe_2B}[x(t)]/dx\}_{x=v}$, and
$J_{Fe}(x=v+dv)=-\{D_{Fe}dC_{Fe}[x(t)]/dx\}_{x=v+dv}$ respectively.

Considering that the boron solubility in the γ phase has a small value ($\approx$ 0 mol m⁻³) in comparison with the lower limit ($C_{low}^{Fe_2B}$) of the boron amount in Fe₂B (= 59.8×10³ mol m⁻³), the output flux can be neglected (J_{Fe} ($x = v + dv$) = $-\{D_{Fe}dC_{Fe}[x(t)]/dx\}_{x=v+dv} \approx 0$). Given these conditions, Equation 4 corresponds to the mass-balance equation and can be rewritten as:

$$\left(\frac{C_{up}^{Fe_2B}+C_{low}^{Fe_2B}-2C_0}{2}\right)\frac{dx(t)}{dt}\bigg|_{x(t)=v} = \tag{5}$$
$$=-D_{Fe_2B}\frac{dC_{Fe_2B}[x(t)]}{dx(t)}\bigg|_{x(t)=v}$$

Using the chain rule on the right term of Equation 5 results in:

$$\left(\frac{C_{up}^{Fe_2B}+C_{low}^{Fe_2B}-2C_0}{2}\right)\frac{dx(t)}{dt}\bigg|_{x(t)=v} = \tag{6}$$
$$=-D_{Fe_2B}\left(\frac{dC_{Fe_2B}[x(t)]}{dt}\right)\left(\frac{dt}{dx(t)}\right)\bigg|_{x(t)=v}$$

Hence, rearranging Equation 6 yields:

$$\left(\frac{C_{up}^{Fe_2B}+C_{low}^{Fe_2B}-2C_0}{2}\right)\left(\frac{dx(t)}{dt}\right)^2\bigg|_{x(t)=v} dt = \tag{7}$$
$$=-D_{Fe_2B}dC_{Fe_2B}[x(t)]\big|_{x(t)=v}$$

Incorporating the parabolic growth law ($v=x(t)=2\varepsilon D_{Fe_2B}^{1/2}t^{1/2}$) on the left term of Equation 7, Equation 8 is obtained:

$$\left(\frac{C_{up}^{Fe_2B}+C_{low}^{Fe_2B}-2C_0}{2}\right)\varepsilon^2\frac{dt}{t} = \tag{8}$$
$$=-dC_{Fe_2B}[x(t)]\big|_{x(t)=v}$$

A schematic representation of the square of the layer thickness against the linear time is depicted in **Figure 3**. Now, we integrate both sides of Equation 8 between the limits of $t_0^{Fe_2B}$ to t and $C_{up}^{Fe_2B}$ to $C_{low}^{Fe_2B}$, respectively:

$$\left(\frac{C_{up}^{Fe_2B}+C_{low}^{Fe_2B}-2C_0}{2}\right)\varepsilon^2\int_{t_0^{Fe_2B}}^{t}\frac{dt}{t} = \tag{9}$$
$$=-\int_{C_{up}^{Fe_2B}}^{C_{low}^{Fe_2B}}dC_{Fe_2B}[x(t)]\big|_{x(t)=v}$$

The following solution is derived:

$$\varepsilon^2 = 2\frac{\left(\dfrac{C_{up}^{Fe_2B}-C_{low}^{Fe_2B}}{C_{up}^{Fe_2B}+C_{low}^{Fe_2B}-2C_0}\right)}{\ln\left(\dfrac{t}{t_0^{Fe_2B}}\right)} \tag{10}$$
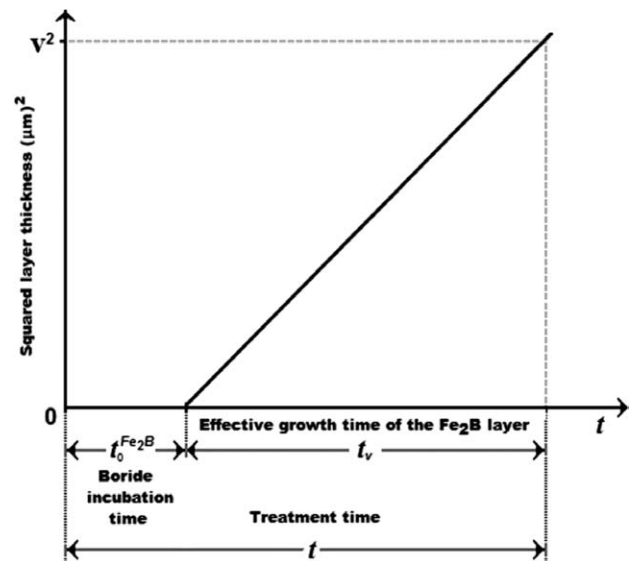
**Figure 3:** Schematic representation of the square of the Fe₂B layer thickness against the treatment time
Slika 3: Shematski prikaz odvisnosti korena debeline plasti Fe₂B od časa obdelave

where ε is known as the normalized growth parameter for the (Fe_2B/substrate) interface, having no physical dimensions. It is assumed that expressions $C_{up}^{Fe_2B}$, $C_{low}^{Fe_2B}$, and C_0 do not depend significantly on the temperature (in the temperature range applied).[10]

3 EXPERIMENTAL PROCEDURE

3.1 Boriding process

Gray cast iron, class 30, complying with the ASTM A-48 standard was employed. Cubic samples with the dimensions of 10 mm × 10 mm × 10 mm of the alloy with the chemical composition of 3.44–3.45 % C, 1.7–1.77 % Si, 0.5–0.6 % Mn, 0.2 % Cr, and 0.45–0.5 % Cu were prepared. Prior to boriding the specimens were polished, ultrasonically cleaned in an alcohol solution in deionized water for 15 min at room temperature, dried and stored under clean-room conditions. The resulting microstructure of the gray cast iron after the solution treatment is presented in **Figure 4a**. It consists of graphite flakes (**Figure 4b**) and a pearlitic matrix with the mean hardness of approximately 316 HV$_{0.05}$.
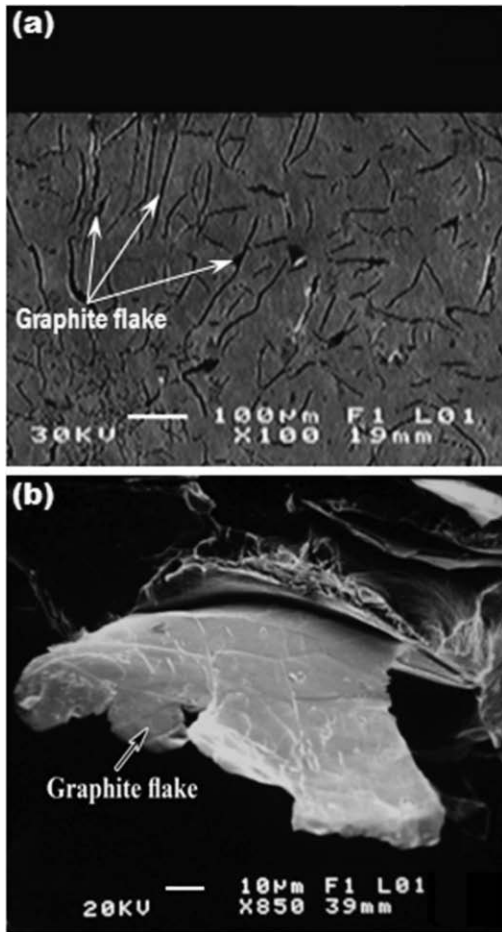

Figure 4: a) Microstructure of gray cast iron after solution treatment, b) SEM micrograph of a graphite flake
Slika 4: a) Mikrostruktura sivega litega železa po raztopnem žarjenju, b) SEM-posnetek grafitnega lističa
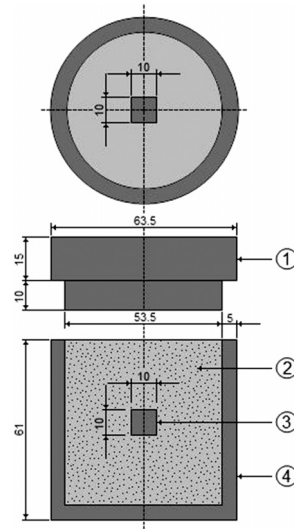
Figure 5: Schematic view of the stainless steel AISI 304L container for the powder-pack boriding treatment: 1 – lid; 2 – powder boriding medium (B_4C + KBF_4 + SiC); 3 – sample; 4 – container
Slika 5: Shematski prikaz posode iz nerjavnega jekla AISI 304L za boriranje s prahom v paketu; 1 – pokrov; 2 – prašnati medij za boriranje (B_4C + KBF_4 + SiC); 3 – vzorec; 4 – posoda

The samples were embedded in a closed cylindrical case (AISI 304L) as shown in **Figure 5**, containing a Durborid fresh-powder boriding medium with the average size of 30 μm (**Figure 6**), consisting of an active boron source (B_4C), an inert filler (SiC) and an activator (KBF_4). The boron potential was controlled with the powder quantity placed over and around the material surface.

The powder-pack boriding was performed in a conventional furnace under a pure argon atmosphere. It is important to note that the oxygen-bearing compounds adversely affect the boriding process[1]. The temperatures of (1123, 1173, 1223, and 1273) K for (2, 4, 6 and 8) h were selected. The boriding temperatures were selected in accordance with the position of the solidus line in the Fe-B phase diagram. Once the treatment was completed, the container was removed from the furnace and slowly
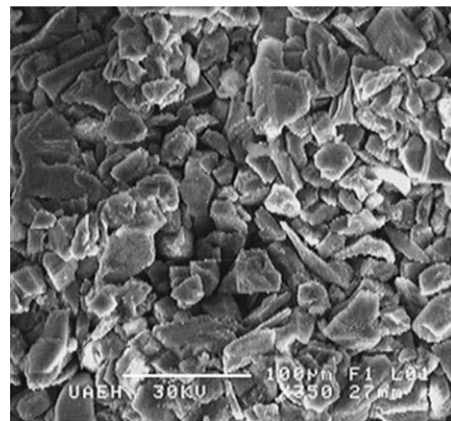

Figure 6: SEM image of boriding powder (B_4C + KBF_4 + SiC)
Slika 6: SEM-posnetek prahu za boriranje (B_4C + KBF_4 + SiC)

cooled to room temperature. After the preliminary experiments it was estimated that the boriding started approximately $\approx$ 31 min after transferring a specimen to the furnace; after that, the so-called boride incubation time set in.

3.2 Characterization of boride layers

The boride samples were cross-sectioned for metallographic examinations using a LECO VC-50 precision-
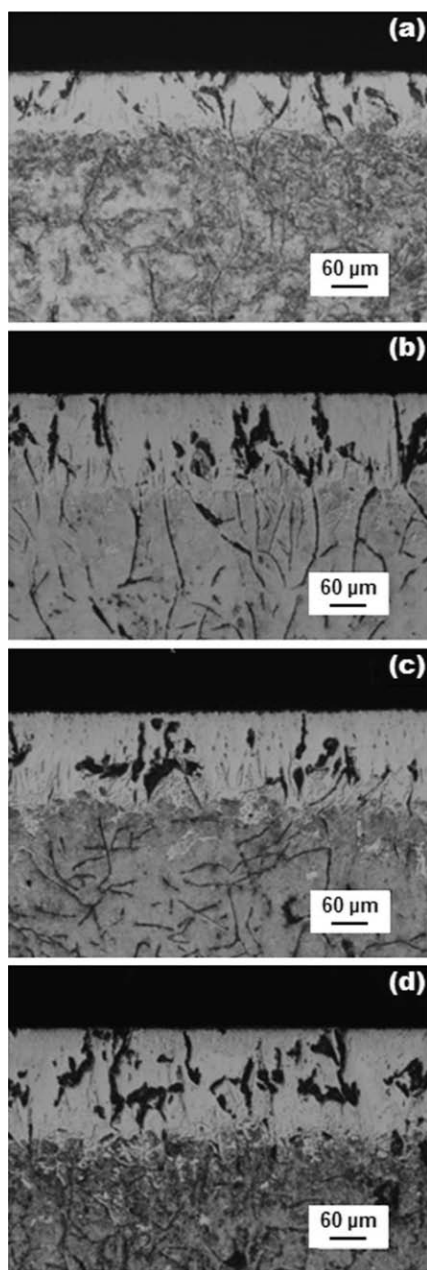
Figure 7: Light micrographs of the Fe₂B layers formed at the surface of the borided ASTM A-48 alloy at 1223 K with the exposure times of: a) 2 h, b) 4 h, c) 6 h and d) 8 h
**Slika 7:** Svetlobni mikroskopski posnetki plasti Fe₂B, nastale na površini borirane zlitine ASTM A-48 pri 1223 K in trajanju: a) 2 h, b) 4 h, c) 6 h in d) 8 h

cutting machine and the depths of the surface layers were observed in a clear field with light microscopy using a GX51 Olympus instrument. **Figure 7** depicts the growth of the Fe₂B layers at the surface of the borided gray cast iron for a particular boriding temperature (1223 K). The images were then analyzed with the MSQ PLUS software.

The thickness measurement program is designed to measure the thickness of layers. The measurement of the layer thickness is exceedingly crucial for the study of the boride-layer growth kinetics. Automatic measurements can be performed by constructing a series of parallel section lines combined with a thresholded image of the layer to be measured. The lengths of those portions of the section lines that overlay the selected layer are measured. In order to minimize the roughness effect on the interface growth, the layer thickness was defined as the average value of the long boride teeth[2,9,14,18,23,25]. Fifty measurements were collected in different sections of the ASTM A-48 borided samples to estimate the thickness of the Fe₂B layers.

All the thickness measurements were collected from a fixed reference on the surface of a borided specimen, as shown in **Figure 8**.

The presence of the iron boride formed at the surface of the sample was verified with X-ray diffraction (XRD), using the equipment (Equinox 2000) with Co K_α radiation at λ = 0.179 nm. The distribution of the alloying elements in a boride layer on gray cast iron was determined with electron dispersive spectroscopy (EDS) (JEOL JSM 6300 LV) from the surface. A Daimler-Benz Rocwell-C adhesion test was employed to assess the adhesion of boride layers. The Rockwell-C indentation test is prescribed by the VDI 3198 norm as a destructive quality test of coated compounds.[32–34] The principle of this method is found in the reference work.[34] A load of 1471 N was applied to cause coating damage adjacent to the boundary of the indentation. Three indentations were conducted for each specimen and scanning electron microscopy (SEM) was employed to evaluate the results.
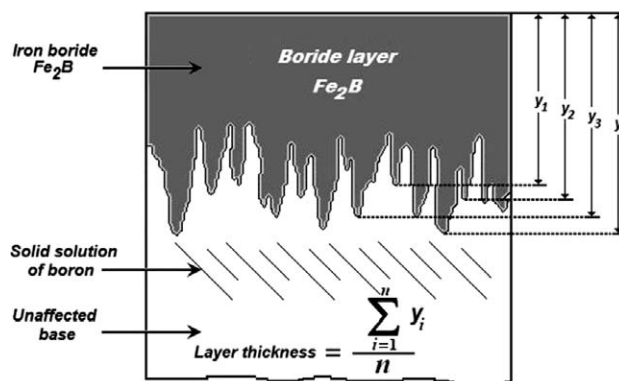

Figure 8: Schematic diagram illustrating the procedure of estimating the boride-layer thickness in gray cast iron
**Slika 8:** Shematski prikaz postopka določanja debeline plasti borida na sivem litem železu

4 RESULTS AND DISCUSSIONS

4.1 Formation mechanism of the borided layer

In the powder-pack boriding, the in-diffusion of atomic boron leads to the formation of borided case structures displaying a boron amount gradient. It is important to recall the overall chemical reaction that takes place during the powder-pack boriding process, i.e.:

$$B_4C + 4KBF_4 + 3SiC + 2O_2 \rightarrow$$
$$\rightarrow 8B \text{ (adsorption)} + 4KF + 3SiF_4 + 4CO \qquad (11)$$
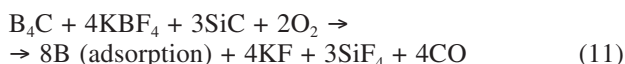
The presence of oxygen promotes oxidation of active boron and Equation (11) will be changed to Equation (12):

$$B_4C + 4KBF_4 + 3SiC + 2O_2 \rightarrow$$
$$\rightarrow 6B \text{ (adsorption)} + 4KF + 3SiF_4 + 4CO + B_2O_2 \quad (12)$$
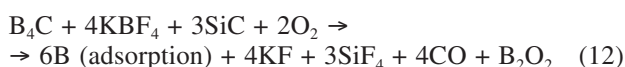
The powder-pack boriding is best done in an inert gas of Ar or N_2. Argon (welding-grade argon is sufficient), unlike nitrogen, has a higher specific weight than air. Therefore, it is more able to drive out oxygen and carbon dioxide from the retort and, for this reason, it is more suitable for use as the inert gas than nitrogen or forming gas. All carbon-dioxide- and carbon-monoxide-bearing gases as well as damp inert gas are unsuitable. The surface of a sample is exposed to the gaseous atmosphere of the atomic boron released from the chemical reaction (Equations 11 and 12) into the substrate, and all the chemical connections (metallic) of the constituent atoms (Fe) are satisfied. However, by definition, the surface represents a discontinuity of those connections. For these incomplete connections, it is strongly favorable to react with the atomic boron that is available, and for that reason it takes place in a spontaneous form. The exact nature of the connection depends on the specimen specificity, but the adsorbed material is generally classified as a chemisorbed material. It can be defined as the concentration (C_{ads}^{B}) of the solute (boron atoms) on the surface of a sample (**Figure 1**). If the boron concentration is in the composition range of $C_{low}^{Fe_2B} < C_{up}^{Fe_2B} < C_{ads}^{B}$, by reacting with active boron atoms B from Equations (11) and (12), the Fe phase can transform into the Fe_2B phase (B(adsorption) + 2Fe $\rightarrow$ Fe_2B). The growth dynamics of the boride coating will be described, distinguishing between the three subsequent stages. During the first stage, it corresponds to the normal diffusion process, which takes place before the formation of the Fe_2B layer. To this period, labeled as time $t_0^{Fe_2B}$ in **Figure 1**, the initial Fe_2B layer (v_0) and the concentration profile ($f(x)$) are associated. The nucleation of the iron boride at the gas-solid interface is the net result of the competition between the supply of boron from the gas phase and the removal of boron due to diffusion into the substrate. During the second stage, significant amounts of Fe_2B crystals form and grow inside, towards the metal bulk. During the third stage, all Fe_2B crystals form and grow inside assuming the preferred crystallographic orientation. Because the growth of the saw-toothed boride layer is a controlled diffusion process with a highly anisotropic nature, higher temperatures and/or longer times stimulate the Fe_2B crystals to make contact with the adjacent crystals and force them to retain the acicular shape[35]. A. J. Ninham and I. M. Hutchings[36] suggested that the columnar nature of the coating interface is caused by a dendrite "side-arm" growth similar to the growth that occurs during the solidification of many metallic systems. In borided low-carbon steels, the boride may "break through" the band of impurities in some places, which allows a rapid local boride growth and results in the characteristic saw-toothed interface. A different mechanism was also proposed, in which local high-stress fields and lattice distortions near the tips of the first acicular nuclei of the reaction products are assumed to be responsible for the columnar growth of borides[37].

4.2 Characterization of boride coatings

A SEM micrograph of the cross-section of the gray cast iron, borided at a temperature of 1123 K for 6 h, is shown in **Figure 9a**. The EDS analysis obtained with SEM is depicted in **Figure 9b**. The results show that chromium dissolves in Fe_2B due to the atomic radius of Cr (= 0.166 nm) which is only a little larger than that of
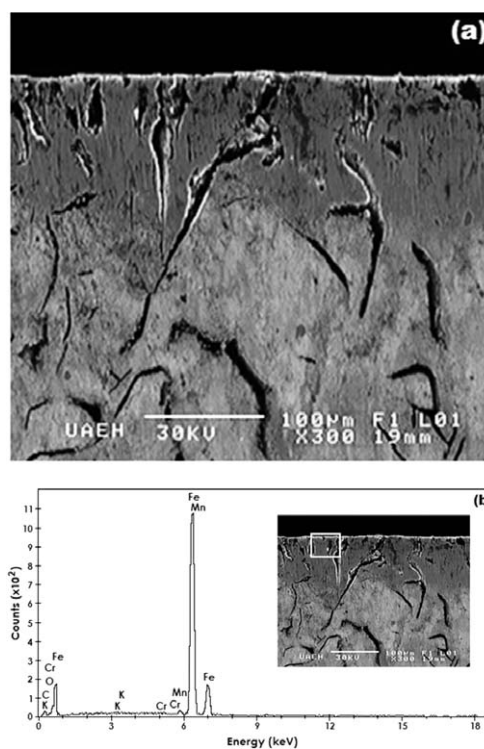

Figure 9: a) Micrograph image of the microstructure of the gray-cast-iron boride layer obtained at 1123 K after an exposure time of 6 h, b) EDS spectrum of a borided sample
Slika 9: a) Mikrostruktura boridne plasti na sivem litem železu, nastale pri 1123 K po 6 h, b) EDS-spekter boriranega vzorca

Fe (= 0.155 nm). It can be expected that Cr replaces Fe in the lattice of boride.

Manganese appears to have a lower solubility. Thus, a deficiency of manganese results in a negative effect on the boride layer in terms of both thickness and morphology. Carbon and silicon do not dissolve significantly across the phase and they do not diffuse through the boride layer, being displaced to the diffusion zone and forming, together with boron, solid solutions like silicoborides (FeSi$_{0.4}$B$_{0.6}$ and Fe$_5$SiB$_2$) and boron-cementite (Fe$_3$B$_{0.67}$C$_{0.33}$)[10,38].

4.3 X-ray diffraction analysis

The presence of Fe$_2$B layers was verified with XRD patterns, as shown in **Figure 10**, in the boundary zones of the borided layers, where it is normally possible to find mixed crystals of different phases. The crystals of the Fe$_2$B type orientate themselves with the *z*-axis perpendicular to the surface. Consequently, the peaks of the Fe$_2$B type phases corresponding to crystallographic planes, with a deviation from zero of the *l* index, show increased intensities in the X-ray diffraction spectra[39].

The growth of boride layers is a controlled diffusion process with a highly anisotropic nature. In the Fe$_2$B phase, the crystallographic direction [001] is the easiest path for the boron diffusion in the body-centered tetragonal lattice of the Fe$_2$B phase, due to the tendency of boride crystals to grow along the direction of minimum resistance, perpendicular to the external surface. As the metal surface is covered, an increasing number of Fe$_2$B crystals come in contact with the adjacent crystals, being forced to grow inside the metal and retaining an acicular shape[35]. The studies on borided cast irons determined the presence of FeB/Fe$_2$B layers at a sample surface[40–43].
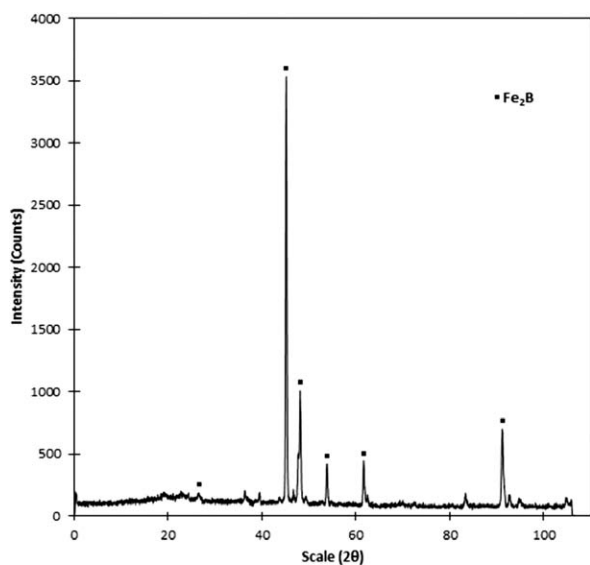
Figure 10: XRD patterns obtained for the surface of the borided ASTM A-48 gray cast iron at 1273 K after 8 h of treatment
Slika 10: XRD-posnetek površine boriranega sivega litega železa ASTM A-48 pri 1273 K po 8 h obdelave
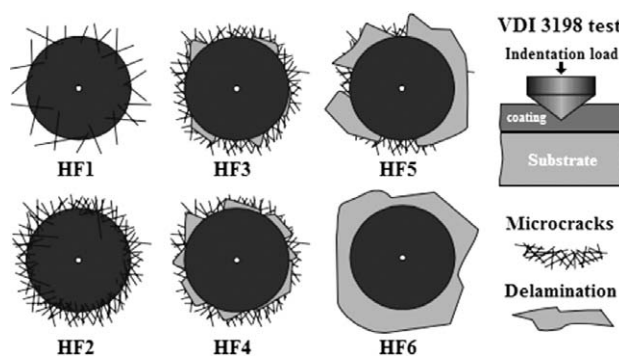

Figure 11: Principle of the VDI 3198 indentation test[32]
Slika 11: Princip VDI 3198-preizkusa z vtiskovanjem[32]

Here, the boron source that provides the boron potential, surrounding the material surface, seems to have influenced the formation of one phase, and only reaches the concentration limits at the surface to create the Fe$_2$B phase. It is known that the media with a low or intermediate boron potential (as compared to the more powerful ones) allow the formation of single Fe$_2$B layers[12,44,45]. In industrial applications, it is desirable to have only the Fe$_2$B phase instead of FeB/Fe$_2$B layers due to significant differences between the expansion coefficients for both phases, which can accelerate the formation of cracks induced by internal stresses.

4.4 Rockwell-C adhesion

For a destructive test of the adhesion of the examined layers a Daimler-Benz Rockwell-C indenter hardness
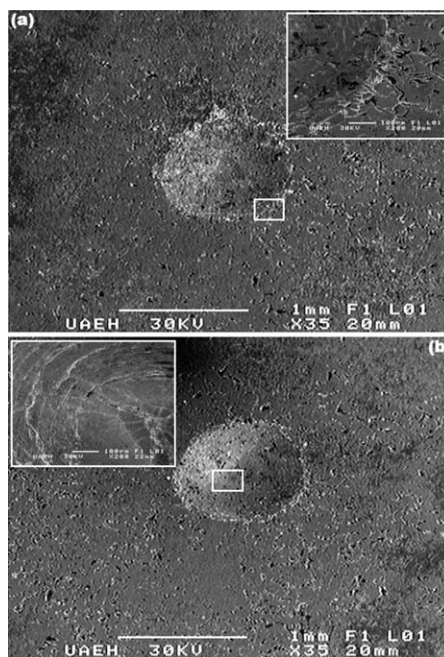
Figure 12: SEM micrographs: a) adjacent to the boundary of the indentation and b) center of the indentation of the VDI adhesion test on gray cast iron
Slika 12: SEM-posnetka VDI-preizkusa adhezije na sivem litem železu: a) v bližini meje vtiska in b) v sredini vtiska
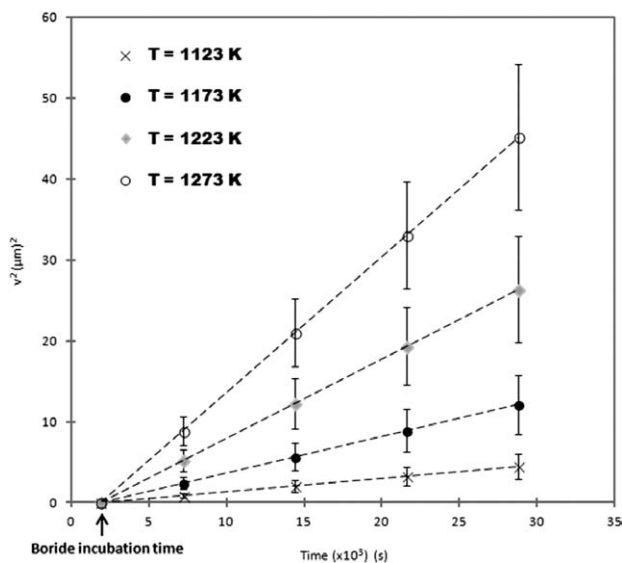
tester was employed, prescribed by the VDI 3198 norm[32]. The principle of this method is presented in **Figure 11**. A conical diamond indenter penetrates into the surface of the investigated layer, inducing a massive plastic deformation of the substrate and fracture of the boride layer. The damage of the boride layer was compared with the adhesion-strength quality maps HF1-HF6 (**Figure 11**). In general, the adhesion strengths HF1 to HF4 define a sufficient adhesion, whereas HF5 and HF6 represent an insufficient adhesion (HF is the German abbreviation for adhesion strength)[32].

Scanning electron microscopy (SEM) images of the indentation craters for the samples borided at 1273 K for 4 h are given in **Figure 12**. The indentation craters obtained on the surface of the borided gray cast iron revealed radial cracks at the perimeters of indentation craters. However, a small quantity of spots with delamination flakes was visible and the adhesion-strength quality of this boride layer corresponded to the HF3 standard.

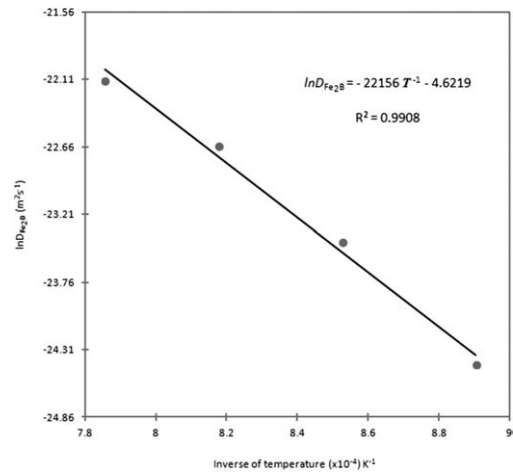### 4.5 Growth kinetics of boride layers

The thickness growth of boride layers as a function of the exposure time is depicted in **Figure 13**. The slopes of the straight lines in **Figure 13** represent the growth constants (= $4\varepsilon^2 D_{Fe_2B}$) of the parabolic growth law ($v^2 = 4\varepsilon^2 D_{Fe_2B}t$), where the intercept on the abscissa is taken as the boride incubation time on the graph.

The results summarized in **Table 1** reflect the diffusion-controlled growth of the boride layers. By combining the results (square of normalized growth parameter (ε^2) and growth constants ($4\varepsilon^2 D_{Fe_2B}$) presented in **Table 1**, the boron diffusion coefficient for the Fe₂B layers (D_{Fe_2B}) was estimated for each boriding temperature.

Figure 14: Boron diffusion coefficient (D_{Fe_2B}) as a function of the boriding temperature
Slika 14: Difuzijski koeficient bora (D_{Fe_2B}) v odvisnosti od temperature boriranja
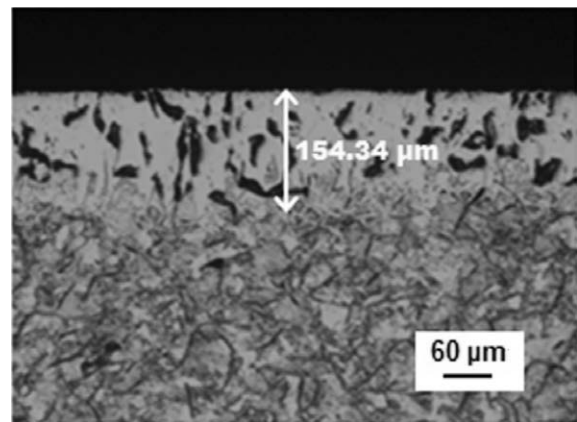
Table 1: Square of normalized growth parameter and growth constants as a function of the boriding temperature
Tabela 1: Kvadrat parametra normalizirane rasti in konstante rasti kot funkcija temperature boriranja

Temperature (K)	Type of layer	ε^2 (Dimensionless)	$4\varepsilon^2 D_{Fe_2B}/$ ($\mu m^2 s^{-1}$)
1123			1.66×10^{-1}
1173	Fe₂B	1.689625×10^{-3}	4.52×10^{-1}
1223			9.81×10^{-1}
1273			16.8×10^{-1}

The activation energy (Q_{Fe_2B}) and the pre-exponential factor (D_0) calculated from the slopes and intercepts of the straight line, shown in coordinate system ln D_{Fe_2B} as a function of the reciprocal boriding temperature is presented in **Figure 14**. The linear relationship is assumed (with the correlation factor of 0.9908):

$$D_{Fe2B} = 9.8\times10^{-3} \exp(-184.2 \text{ kJ mol}^{-1} / RT) \quad (13)$$

Figure 13: Square of the Fe₂B layers thickness (v^2) versus boriding time (t) at different temperatures
Slika 13: Odvisnost kvadrata debeline plasti Fe₂B (v^2) od časa boriranja (t) pri različnih temperaturah

Figure 15: Light micrograph of the boride layer formed on gray cast iron during the powder-pack boriding at 1253 K after an exposure time of 5 h
Slika 15: Svetlobni posnetek mikrostrukture boridne plasti na sivem litem železu pri boriranju s prahom v paketu pri 1253 K in trajanju 5 h

where $R = 8.3144621$ J mol^{-1} K^{-1} and T is the absolute temperature (K). According to Equation 13, the pre-exponential factors and the activation-energy values are affected by the contact surface between the boriding medium and the substrate, as well as the chemical composition of the material[12,17]. The growth kinetics of boride layers obtained with the diffusion model was verified by estimating the Fe₂B layer thickness as a function of the temperature and exposure time.

Figure 15 shows a light image of the boride layer formed at 1253 K after 5 h of treatment. With Equation 14, the boride-layer thicknesses are described as follows:

$$v = 2\varepsilon D_{\mathrm{Fe_2B}}^{1/2} t^{1/2} = \sqrt{\frac{8 D_{\mathrm{Fe_2B}} t (C_{\mathrm{up}}^{\mathrm{Fe_2B}} - C_{\mathrm{low}}^{\mathrm{Fe_2B}})}{\ln(t/t_0^{\mathrm{Fe_2B}})(C_{\mathrm{up}}^{\mathrm{Fe_2B}} + C_{\mathrm{low}}^{\mathrm{Fe_2B}} - 2C_0)}} \quad (14)$$

As depicted in **Table 2,** the results obtained from Equation 14 exhibit a good agreement between the experimental data and the theoretical results.

Table 2: Estimated value of the gray-cast-iron boride-layer thickness (v) obtained at a boriding temperature of 1253 K with an exposure time of 5 h

Tabela 2: Izmerjene debeline (v) plasti borida na sivem litem železu, nastale pri 1253 K in trajanju boriranja 5 h

Temperature (K)	Type of layer	Boride-layer thickness (µm) estimated with Eq. 14	Experimental boride-layer thickness (µm)
1253	Fe₂B	148.34	154.34±16.52

The Fe₂B layer thicknesses for the set of experimental parameters of the borided gray cast iron are presented with contour plots as functions of the temperature and exposure time as shown in **Figure 16**. Hence, Equation 14 can be used to estimate the optimum boride-layer
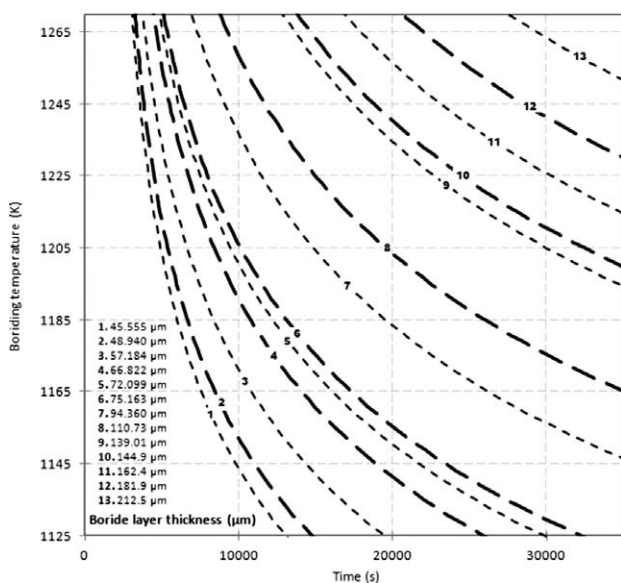
Figure 16: Contour diagram for the estimation of process parameters and layer thickness

Slika 16: Diagram obrisov debeline plasti za določanje parametrov procesa

thicknesses for the borided gray cast iron. It is a standard practice to match the case depth with the intended industrial application and the base material.

As a rule, thin layers (e.g., 15–20 µm) are used to protect against adhesive wear (associated with chipless shaping and metal-stamping dies and tools), whereas thick layers are recommended for combating abrasive wear (extrusion tooling for plastics with abrasive fillers and pressing tools for the ceramic industry). In the case of low-carbon steels and low-alloy steels, the optimum boride-layer thickness ranges from 50 µm to 250 µm, and for high-alloy steels, the optimum boride-layer thickness ranges from 25 µm to 76 µm. In addition, this model can be extended to predict the growth kinetics of FeB/Fe₂B boride coatings on the surfaces of different ferrous alloys.

5 CONCLUSIONS

The growth kinetics of a boride layer (Fe₂B) on gray cast iron was evaluated with a mathematical model. The boride incubation time was taken into account for the powder-pack boriding and the main assumptions were adopted on the basis of reference[10]. The dependence between the boron diffusion coefficients and the boriding temperature was expressed with the Arrhenius equation for the temperature range of 1123–1273 K. An empirical equation was derived to predict the thickness of the boride layer for the temperatures between 1123 K and 1273 K with the boriding times between 2 h and 8 h. The validity of the diffusion model was tested by comparing the thickness of the experimental boride layer obtained with boriding 5 h with that deduced using the model (see Equation 14). On the other hand, the adhesion-strength quality of the boride layer formed on the surface of gray cast iron is estimated as HF3 after 4 h of boriding at 1273 K. The large differences or mismatches in the coefficients of the thermal expansion of Fe₂B ($\alpha_{\mathrm{Fe_2B}} = 2.9 \times 10^{-8}$ K^{-1}) and Fe ($\alpha_{\mathrm{Fe}} = 0.11 \times 10^{-8}$ K^{-1}) may have also played some roles in the large-scale delamination and flaking off the top Fe₂B layer. The contour diagram, which can be used for future applications of borided gray cast iron, was developed not only to estimate the thickness of a boride layer with the used process parameters but also to predict the process parameters on the basis of the thicknesses of boride layers.

Desarrollo Curricular y NuevosProductos and VicerrectoríaAcadémica UNITEC for all the facilities to accomplish this research work.

Nomenclature

α_{FeB} – thermal expansion coefficient of the FeB layer (K^{-1})

α_{Fe_2B} – thermal expansion coefficient of the Fe₂B layer (K^{-1})

v – boride layer thickness (m)

k_{Fe_2B} – rate constant in the Fe₂B phase $(m\ s^{-1/2})$

t_v – effective growth time of the Fe₂B layer (s)

t – treatment time (s)

$t_0^{Fe_2B}$ – boride incubation time (s)

Q_{Fe_2B} – activation energy of the system $(J\ mol^{-1})$

$C_{up}^{Fe_2B}$ – upper limit of boron amount in Fe₂B $(60 \times 10^3$ mol m$^{-3})$

$C_{low}^{Fe_2B}$ – lower limit of boron amount in Fe₂B $(59.8 \times 10^3$ mol m$^{-3})$

C_{ads}^{B} – adsorbed boron concentration in the boride layer (mol m^{-3})

$a_1 = C_{up}^{Fe_2B} - C_{low}^{Fe_2B}$ – homogeneity range of the Fe₂B layer (mol m^{-3})

$a_2 = C_{low}^{Fe_2B} - C_0$ – miscibility gap (mol m^{-3})

C_0 – terminal solubility of the interstitial solute (≈ 0 mol m^{-3})

$C_{Fe_2B}\ [x(t)]$ – boron concentration profile for the Fe₂B layer (mol m^{-3})

v_0 – initial Fe₂B layer (m)

ε – normalized growth parameter for the (Fe₂B/substrate) interface (it has no physical dimensions)

D_{Fe_2B} – diffusion coefficient of boron in the Fe₂B phase $(m^2\ s^{-1})$

$J_i[x(t)]$, (with i = Fe₂B and Fe) – boron atom fluxes in the (Fe₂B/substrate) interface (mol m$^{-2}\ s^{-1}$)

6 REFERENCES

[1] G. Wahl, Boronizing, Durferrit-Technical Information, Reprint from VDI-Z117, Germany 1975, 785–789

[2] A. Graf von Matuschka, Boronizing, 1st ed., Carl Hanser Verlag, Munich 1980

[3] J. R. Davis, Surface Hardening of Steels, Understanding the Basics, ASM International, USA 2002, 213–223

[4] S. C. Singhal, Thin Solid Films, 45 (**1977**), 321–329

[5] K. Genel, I. Ozbek, C. Bindal, Materials Science and Engineering, A347 (**2003**), 311–314

[6] U. Yapar, C. F. Arýsoy, G. Basman, S. A. Yesilcubuk, M. K. Sesen, Key Engineering Materials, 264–268 (**2004**), 633–636

[7] W. Fichtl, Rev. Int. Hautes Temper, 17 (**1980**), 33–43

[8] I. Campos-Silva, M. Ortiz-Domínguez, N. López-Perrusquia, A. Meneses-Amador, R. Escobar-Galindo, J. Martínez-Trinidad, Applied Surface Science, 256 (**2010**), 2372–2379

[9] M. Kulka, N. Makuch, A. Pertek, L. Maldzinski, Journal of Solid State Chemistry, 199 (**2013**), 196–203

[10] C. M. Brakman, A. W. J. Gommers, E. J. Mittemeijer, J. Mater. Res., 4 (**1989**), 1354–1370

[11] S. Sen, U. Sen, C. Bindal, Vacuum, 77 (**2005**), 195–202

[12] I. Campos, O. Bautista, G. Ramírez, M. Islas, J. De La Parra, L. Zúñiga, Applied Surface Science, 243 (**2005**), 431–438

[13] L. G. Yu, X. J. Chen, K. A. Khor, G. Sundararajan, Acta Materialia, 53 (**2005**), 2361–2368

[14] I. Campos, R. Torres, O. Bautista, G. Ramírez, L. Zuñiga, Applied Surface Science, 252 (**2006**), 2396–2403

[15] O. Ozdemir, M. Usta, C. Bindal, A. H. Ucisik, Vacuum, 80 (**2006**), 1391–1395

[16] X. J. Chen, L. G. Yu, K. A. Khor, G. Sundararajan, Surface and Coatings Technology, 202 (**2008**), 2830–2836

[17] I. Campos-Silva, M. Ortiz-Dominguez, H. Cimenoglu, R. Escobar-Galindo, M. Keddam, M. Elias-Espinosa, N. López-Perrusquia, Surface Engineering, 27 (**2011**), 189–195

[18] I. Campos-Silva, M. Ortiz-Domínguez, O. Bravo-Bárcenas, M. A. Doñu-Ruiz, D. Bravo-Bárcenas, C. Tapia-Quintero, M. Y. Jiménez-Reyes, Surface and Coatings Technology, 205 (**2010**), 403–412

[19] M. Keddam, M. Ortiz-Domínguez, I. Campos-Silva, J. Martínez-Trinidad, Applied Surface Science, 256 (**2010**), 3128–3132

[20] I. Gunes, Bulletin of Materials Science, 38 (**2013**), 527–541

[21] I. Campos-Silva, M. Flores-Jiménez, G. Rodríguez-Castro, E. Hernández-Sánchez, J. Martínez Trinidad, R. Tadeo-Rosas, Surface and Coatings Technology, 237 (**2013**), 429–439

[22] I. Campos-Silva, M. Ortiz-Domínguez, C. Villa Velazquez, R. Escobar, N. López, Defect and Diffusion Forum, 272 (**2007**), 79–86

[23] M. Ortiz Domínguez, Contribución de la Modelación Matemática en el Tratamiento Termoquímico de Borurización, PhD thesis, SEPI-ESIME from the Instituto Politécnico Nacional, México, 2013

[24] M. Keddam, S. M. Chentouf, Applied Surface Science, 252 (**2005**), 393–399

[25] I. Campos-Silva, D. Bravo-Bárcenas, A. Meneses-Amador, M. Ortiz-Dominguez, H. Cimenoglu, U. Figueroa-López, J. Andraca-Adame, Surface and Coatings Technology, 237 (**2013**), 402–414

[26] T. B. Massalski, Binary Alloy Phase Diagrams, ASM International, Materials Park, Ohio 1990, 280

[27] H. Okamoto, Journal of Phase Equilibria and Diffusion, 25 (**2004**), 297–298

[28] V. I. Dybkov, Reaction Diffusion and Solid State Chemical Kinetics, Trans Tech Publications, Switzerland-UK-USA 2010, 7

[29] W. Jost, Diffusion in Solids, Liquids, Gases, Academic Press Inc, New York 1960, 69–72

[30] P. Shewmon, Diffusion in Solids, Minerals, Metals and Materials Society, USA 1989, 40

[31] D. A. Porter, K. E. Easterling, Phase Transformations in Metals and Alloys, Chapman and Hall, London 1981, 105

[32] Verein Deutscher Ingenieure Normen VDI 3198, VDI-Verlag, Düsseldorf 1991, 1–8

[33] N. Vidakis, A. Antoniadis, N. Bilalis, J. Mater Process Technol, 143–144 (**2003**), 481–485

[34] S. Taktak, Materials and Design, 28 (**2007**), 1836–1843

[35] G. Palombarini, M. Carbucicchio, Journal of Materials Science Letter, 6 (**1987**), 415–416

[36] A. J. Ninham, I. M. Hutchings, Journal of Vacuum Science and Technology A: Vacuum Surfaces and Films, 4 (**1986**), 2827–2831

[37] M. Carbucicchio, G. Palombarini, Hyperfine Interactions, 83 (**1994**), 91–110

[38] I. S. Dukarevich, M. V. Mozharov, A. S. Shigarev, Metallovedenie Termicheskaya i Obrabotka Metallov, 2 (**1973**), 64–66

[39] C. Badini, D. Mazza, Journal Materials Science Letters, 23 (**1988**), 661–665

[40] U. Sen, S. Sen, F. Yilmaz, Journal of Materials Processing Technology, 148 (**2004**), 1–7

[41] U. Sen, S. Sen, F. Yilmaz, Surface and Coatings Technology, 176 (**2004**), 222–228

[42] S. Sahin, C. Meric, Research Bulletin, 37 (**2002**), 971–979

[43] Y. Yalcin, A. M. Yazici, Kovove Materialy, 45 (**2007**), 51–57
[44] C. Bindal, A. H. Ucisik, Surface and Coatings Technology, 122 (**1999**), 208–213
[45] J. Vipin, G. Sundararajan, Surface and Coatings Technology, 149 (**2002**), 21–26